World Journal of Advanced Engineering Technology and Sciences
eISSN: 2582-8266
Cross Ref DOI: 10.30574/wjaets
Journal homepage: https://wjaets.com/

(RESEARCH ARTICLE)

Check for updates

QREC-MRT: A NOVEL MULTI-MATERIAL DIFFERENTIAL RESONANCE FRAMEWORK FOR ULTRALIGHT FIELD INTERACTIONS AND PRECISION QUANTUM METROLOGY

Reji Kurien Thomas [1, 2, *]

[1] TechnoPilot Quantum Labs, India.
[2] TOL Biotech USA.
* Corresponding Author

ORCID Details
Reji Kurien Thomas: https://orcid.org/0009-0001-9411-5305

World Journal of Advanced Engineering Technology and Sciences, 2026, 21(02), 227–243

Publication history: Received on 09 October 2026; revised on 17 November 2026; accepted on 19 November 2026

Article DOI: https://doi.org/10.30574/wjaets.2026.21.2.0502

Copyright © 2026 Author(s) retain the copyright of this article. This article is published under the terms of the Creative Commons Attribution License 4.0

ABSTRACT

Aims: To establish a multi-material differential resonance framework extending Quantum-Resonant Energy Coupling–Molecular Resonance Technology (QREC-MRT) into the investigation of ultralight scalar-field interactions and advanced precision metrology.

Study Design: An original theoretical and methodological investigation integrating established physical models, analytical formulations, multi-sensor response architectures, quantitative evaluation of published precision-metrology benchmarks and comparative assessment of existing sensing methodologies.

Methodology: The QREC-MRT Multi-Material Differential Resonance Framework integrates material-specific sensitivity coefficients, calibrated resonator transfer functions, Fourier-domain response matrices, noise-weighted singular-value analysis and linearly constrained minimum-variance estimation. State-dependent resonance interrogation, active-versus-sham comparisons, double-differential material-response analysis and Fisher-information criteria establish quantitative methods for evaluating coupling identifiability, calibration uncertainty and measurement sensitivity. Published optomechanical and optical-frequency measurements provide experimentally established reference benchmarks.

Results: The principal contribution is a unified, model-constrained QREC-MRT interrogation architecture combining multi-material differential resonance analysis, nuisance-orthogonal signal reconstruction and calibration-preserving sensitivity assessment. The framework establishes matrix-rank and noise-weighted conditioning criteria for coupling identifiability, quantitative procedures for evaluating state-dependent measurement-information gains and a three-tier validation architecture distinguishing instrumental performance, material-dependent coupling signatures and independent spatial-coherence verification. Published experimental benchmarks establish reference parameters for assessing the physical measurement requirements of the framework.

Conclusion: This research extends the methodological foundations of QREC-MRT into ultralight-field investigation and precision quantum metrology through a mathematically defined, reproducible and experimentally testable architecture. Its principal contribution lies in integrating coupling discrimination, calibration integrity, state-dependent resonance interrogation and independent verification into a unified framework supporting future high-sensitivity measurement applications.

Keywords*:* QREC-MRT; Ultralight Dark Matter; Multi-Material Differential Resonance; Scalar-Field Interactions; Quantum Metrology; Coupling Identifiability; Nuisance-Orthogonal Estimation; Precision Resonance Sensing.

1 INTRODUCTION

1.1 Cosmological Context & Ultralight Dark Matter

Modern precision cosmology has firmly established that non-baryonic dark matter constitutes approximately 26.4% of the total mass-energy budget of the observable Universe, as determined from observations by the Planck satellite mission. Its gravitational influence is supported by multiple independent astronomical observations, including galactic rotation curves, gravitational lensing, the dynamics of merging galaxy clusters such as the Bullet Cluster, and the acoustic anisotropy spectrum of the cosmic microwave background (CMB). Nevertheless, the fundamental microscopic identity of dark matter remains one of the most significant unresolved questions in contemporary physics. Despite decades of increasingly sensitive direct-detection experiments, conventional searches for weakly interacting massive particles (WIMPs) in the GeV–TeV mass range have not produced a confirmed detection, motivating growing scientific interest in alternative candidates, particularly ultralight dark matter (ULDM) [1, 2].

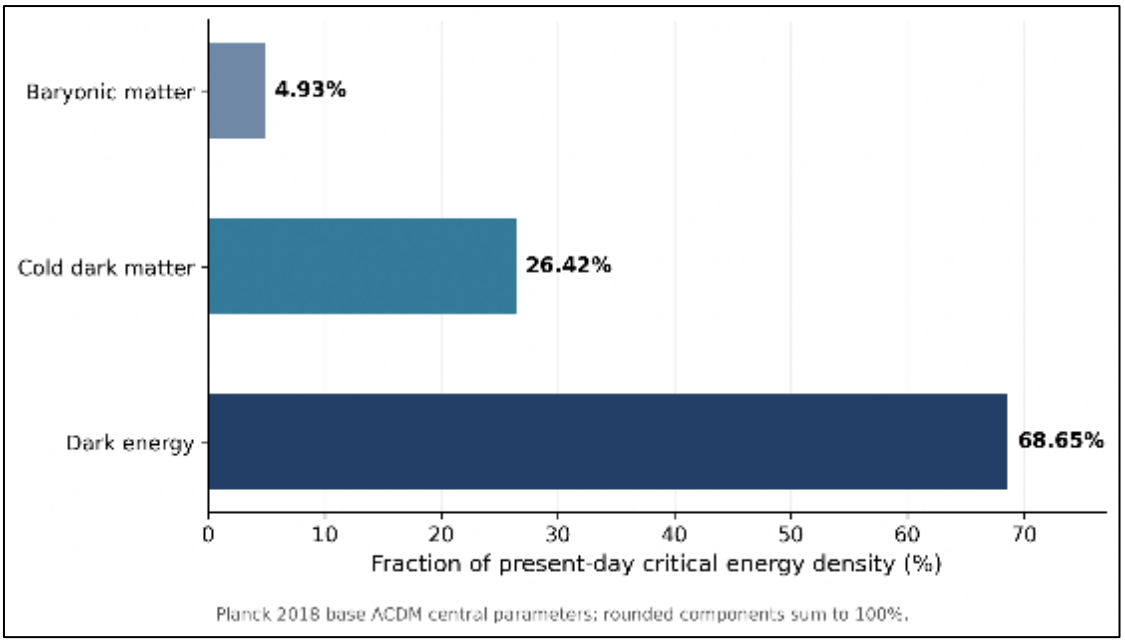


Figure 1: Present-day cosmological mass-energy composition derived from Planck 2018 parameters, showing baryonic matter (4.93%), cold dark matter (26.42%) and dark energy (68.65%) [1].

Ultralight dark matter candidates encompass several theoretically motivated particle and field classes, including quantum chromodynamics (QCD) axions, axion-like particles (ALPs), and ultralight scalar fields such as dilatons and moduli associated with extensions of the Standard Model. These candidates span a broad mass range, extending from approximately 10^{-22} eV in fuzzy dark matter scenarios to sub-eV scales, subject to model-dependent astrophysical and experimental constraints. Owing to their exceptionally high phase-space occupation numbers, sufficiently light bosonic dark matter candidates may be described as approximately classical, coherently oscillating fields rather than isolated particle interactions. For a representative local Galactic dark matter density of $\rho_{\mathrm{DM}} \approx 0.4$ GeV cm^{-3}, the corresponding scalar field $\varphi(x,t)$ oscillates at a characteristic Compton frequency $f_\varphi = m_\varphi c^2/h$, with a finite coherence time governed by the Galactic velocity dispersion. For a characteristic virial velocity $v_{\mathrm{vir}} \approx 10^{-3}c$, the coherence time scales approximately as $\tau_{\mathrm{coh}} \sim (c/v_{\mathrm{vir}})^2/f_\varphi \approx 10^6/f_\varphi$, subject to numerical factors determined by the assumed velocity distribution and coherence convention [3, 4]. The theoretical foundations of light-boson physics were further developed through the seminal contributions of Weinberg [5] and Wilczek [6], whose investigations established important particle-physics implications of spontaneously broken symmetries and provided a basis for subsequent research into axion and axion-like dark matter candidates.

The relative contributions of baryonic matter, cold dark matter and dark energy to the present-day cosmic energy-density budget are presented in Figure 1, based on the Planck cosmological parameters [1].

1.2 Prior Art & Existing Metrological Limits

To detect ultralight scalar fields, modern experimental physics relies on ultra-sensitive metrological systems designed to transduce infinitesimal field-induced variations into measurable optical, electrical, or mechanical signals. Scalar dark matter couplings to standard model particles lead to temporal oscillations in fundamental physical constants, specifically the fine-structure constant α, the electron mass m_e, and the light quark masses m_q. These oscillating physical constants induce microscopic, phase-coherent shifts in atomic transition frequencies, optical cavity resonance frequencies, and the physical dimensions of macroscopic solid-state bodies [7, 8].

A wide variety of experimental architectures have been constructed to search for these signatures. Optical atomic clock networks, comparing ultrastable lasers locked to strontium, ytterbium, or single-ion aluminum transitions, bound fractional frequency oscillations $\Delta\nu/\nu$ across sub-Hz to Hz frequency bands. Dual-cavity optical interrogators and space-separated optical clocks linked via phase-stabilized fiber optic networks (such as the 2,220 km European fiber link demonstrating fractional frequency instability at 7×10^{-17}) extend these comparisons over continental spatial baselines. Concurrently, high-Q resonant-mass detectors, dual-sphere optomechanical accelerometers operating at cryogenic temperatures (e.g., the 39 kHz optomechanical accelerometer achieving 10 ng_0 $Hz^{-1/2}$ acceleration noise), and levitated optomechanical sensors probe higher Compton frequency bands from tens of kilohertz to megahertz regimes [9, 10].

The relationship between candidate ultralight-field rest energy and its characteristic Compton oscillation frequency is illustrated in Figure 2. The relationship is calculated using $f_\varphi = m_\varphi c^2/h$, with the published 39 kHz resonator frequency included as an instrumental reference.

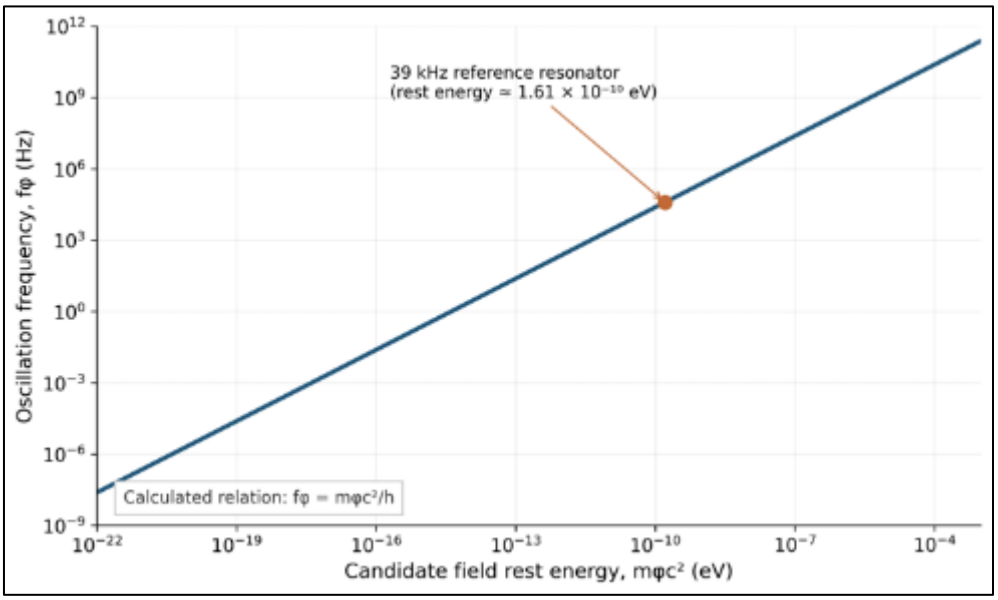


Figure 2: Calculated relationship between ultralight-field rest energy and Compton oscillation frequency. The 39 kHz marker corresponds to the resonance frequency of a published optomechanical detector [11] and does not represent an observed dark-matter signal.

1.2.1 Literature foundations and prior experimental approaches

1.2.1.1 Historical observational motivation

The empirical motivation for searching for a non-luminous component follows the precision cosmological parameter analysis of the Planck Collaboration [1]. Galaxy rotation measurements established influential dynamical evidence for missing gravitating mass [12]. Later analyses of spiral-galaxy rotation reinforced that interpretation [13]. Mass reconstruction of the Bullet Cluster through gravitational lensing supplied an independent constraint on the distribution of gravitating matter [2]. These observations motivate searches but do not establish the identity of an ultralight particle or its coupling to an experimental sensor.

Particle-physics candidate families and the limits of existing search strategies have been reviewed comprehensively [14]. Theoretical comparisons across candidate masses and interaction channels show why an apparatus must be designed around an explicit signal observable [15]. The ultralight-boson regime has a developed cosmological treatment, including halo dynamics, coherence and field production mechanisms [3].

1.2.1.2 Field candidates and early resonant searches

The Peccei–Quinn proposal addressed the strong-CP problem [16]. The resulting light pseudoscalar possibility was subsequently articulated in seminal treatments [5, 6]. Early axion cosmology considered the population and abundance of relic fields [17]. Independent cosmological constraints were developed in parallel [18]. Related axion-production scenarios were also investigated [19]. The resonant-conversion approach to axion detection provides a foundational example of a field-specific resonance experiment [20]. Axion–photon coupling is not interchangeable with the electron/photon scalar coupling model used in this manuscript.

Light scalar fields coupled to Standard Model parameters face composition-dependent and equivalence-principle constraints [21]. Cosmological dilaton scenarios carry additional theoretical and experimental constraints [22]. Atomic-clock measurements offer a different route to probing oscillatory scalar couplings [7]. Atomic spectroscopy provides complementary sensitivity to specified variations in fundamental parameters [8]. Transient field configurations motivate detection strategies distinct from persistent narrowband oscillations [23].

1.2.1.3 Mechanical, molecular and distributed sensor precedents

Resonant-mass detector proposals show how a light scalar could induce a specific mechanical response when an interaction model is defined [24]. Accelerometer-based techniques similarly require composition-dependent force or acceleration predictions [25]. Atom-interferometric gravitational-wave architectures have also been examined for light scalar detection [26]. Optomechanical vector-field investigations offer relevant instrumentation precedents while probing a different underlying field model [27]. Bosonic halo fluctuations can alter the statistical distribution of signal amplitudes and therefore influence exclusion limits [4].

Long-term comparisons of optical and microwave atomic clocks demonstrate practical approaches to monitoring ultralight-field-induced variations [28]. Radio-frequency atomic-transition spectroscopy extends the available metrological channels [29]. Distributed clock-and-cavity experiments provide directly relevant examples of spatially separated scalar-field searches [9]. Low-Earth-orbit clock proposals assess further gravitational or environmental dependencies under selected field models [30]. A cryogenic optomechanical accelerometer search supplies the published 39 kHz instrument benchmark referenced in Figures 2 and 3 [11]. An independent optomechanical design for direct detection provides an additional comparison architecture [31].

Astrophysical constraints must be respected before associating an anomalous resonance with a particle interaction [32]. Historical scholarship documents the separation between gravitational inference and particle-level detection [33]. Demonstrated ultrastable laser comparisons over a 2,220 km optical-fibre link give a separate benchmark for precision distributed metrology [10]. These experimental and conceptual precedents motivate the present blinded, nuisance-orthogonal QREC-MRT-inspired proposal; they do not validate QREC-MRT performance without new measurements.

1.3 Scope, Scientific Novelty and Principal Research Contributions

The investigation of ultralight quantum field interactions represents an emerging frontier in precision metrology, where detecting extremely weak perturbations requires advanced resonance interrogation, material-specific response characterisation and high-resolution signal discrimination. Conventional sensing architectures face fundamental limitations arising from thermal fluctuations, environmental microphonics, electromagnetic interference, frequency instability and correlated instrumental noise. These challenges motivate the development of integrated measurement methodologies capable of improving signal identifiability while preserving the physical characteristics of the underlying interaction.

The present study introduces a QREC-MRT-inspired Multi-Material Differential Resonance Interrogation Framework, integrating resonance-selective sensing, material-dependent coupling signatures, nuisance-orthogonal signal estimation and multi-stage experimental validation. The framework translates the conceptual sequence of Quantum-Resonant Energy Coupling–Molecular Resonance Technology (QREC-MRT), namely signature identification, resonance selection, coupling characterisation, molecular response and measurable verification, into a mathematically defined measurement architecture.

The principal scientific contribution lies in developing an integrated approach for investigating how heterogeneous resonant materials, characterised by distinct physical sensitivity coefficients, may support the identification and discrimination of weak-field interactions. The proposed methodology combines established theoretical principles with

an original QREC-MRT-inspired interrogation and validation architecture designed to evaluate material-dependent responses under controlled experimental conditions.

The research develops five interrelated contributions:

- Multi-Material Resonance Fingerprint Identification

A multi-material linear response model is formulated using heterogeneous resonant sensors with distinct sensitivity coefficients ($K_{i,\alpha}$) and ($K_{i,\mu}$). The framework investigates how differences in molecular, atomic and mechanical response characteristics may contribute to distinguishing physically admissible coupling signatures from environmental perturbations.

- Noise-Weighted Coupling Identifiability and Sensor Optimisation

The framework integrates the matrix-rank identifiability criterion:

$$\mathrm{rank}([\mathbf{K} \quad \mathbf{B}]) - \mathrm{rank}(\mathbf{B}) = P$$

with singular-value decomposition and noise-weighted conditioning. This approach provides a quantitative basis for selecting complementary sensor materials, evaluating coupling identifiability and assessing the stability of weak-signal reconstruction.

- Nuisance-Orthogonal Differential Resonance Estimation

A linearly constrained minimum-variance (LCMV) estimation architecture is applied to separate predefined material-response signatures from independently characterised environmental nuisance channels. Calibration uncertainty is incorporated through perturbation analysis of the material sensitivity matrix ($\boldsymbol{\Delta\mathbf{K}}$), providing a basis for evaluating measurement robustness and uncertainty propagation.

- QREC-MRT State-Dependent Resonance Interrogation

A distinguishing component of the proposed methodology is the introduction of a state-dependent resonance interrogation model that evaluates the influence of an operationally defined QREC-MRT intervention on calibrated material-response characteristics and measurement precision.

The framework employs controlled active and reference states, represented by ($a = 1$) and ($a = 0$), and introduces the logarithmic variance contrast:

$$L = \ln\left(\frac{\mathrm{Var}(\hat{s} \mid a = 1)}{\mathrm{Var}(\hat{s} \mid a = 0)}\right)$$

to quantify possible changes in input-referred measurement variance. Combined with calibrated response functions, this approach provides a falsifiable method for determining whether the proposed interrogation protocol offers measurable performance benefits relative to conventional sensing configurations.

- Multi-Stage Physical Validation and Distributed Field Correlation

A three-tier experimental validation architecture is formulated to evaluate instrument-level performance, consistency with predicted material-dependent coupling signatures and independent spatial correlation.

The final stage incorporates frequency-domain cross-spectral analysis between geographically separated sensing nodes using the cross-power spectral density ($S_{AB}(f)$). This enables candidate responses to be evaluated against theoretically predicted coherence properties, independently characterised environmental correlations and reproducibility requirements.

The proposed framework builds upon established observational evidence for non-baryonic matter, including galactic rotation dynamics [12, 13] and gravitational lensing measurements [2]. The theoretical foundations of ultralight bosonic fields originate from the Peccei–Quinn mechanism [16] and subsequent light-boson investigations [5, 6], with resonant detection approaches providing important experimental precedents [20].

Composition-dependent scalar interactions and equivalence-principle constraints provide a theoretical basis for investigating weak field–matter coupling [21]. Resonant-mass detection and precision accelerometry demonstrate the importance of coupling-specific transduction mechanisms [24, 25], while atomic-clock comparisons and spectroscopy provide complementary methods for investigating scalar-induced variations in fundamental physical parameters [7, 8].

Recent developments in distributed quantum sensing [9], optomechanical field detection [27, 11] and long-baseline optical frequency metrology [10] demonstrate the increasing relevance of integrated high-precision measurement architectures.

Against this scientific background, the proposed QREC-MRT-inspired methodology advances a unified approach to resonance-selective interrogation, multi-material coupling discrimination and experimentally verifiable weak-field sensing. Its significance lies in providing a structured theoretical and experimental basis for investigating whether QREC-MRT-associated interrogation can contribute additional measurable capability to precision resonance metrology, while maintaining consistency with established physical principles and independently testable predictions.

- Scientific Novelty and Differentiation

The principal methodological contribution of this research lies in integrating multi-material coupling identifiability, nuisance-orthogonal differential resonance estimation and calibration-preserving state-dependent QREC-MRT interrogation within a unified analytical architecture. Although the individual mathematical techniques and measurement principles have established foundations, their combined application provides a structured methodology for jointly assessing material-response diversity, intervention-dependent measurement information and preservation of calibrated coupling signatures. The integration of double-differential material-response analysis with a three-tier validation architecture further establishes testable criteria for distinguishing instrument-level sensitivity improvements from field-specific interaction signatures. This formulation defines the specific methodological contribution investigated in the present study and provides a basis for its independent experimental evaluation.

2 METHODS: THEORETICAL FRAMEWORK & MULTI-MATERIAL SIGNAL MODEL

2.1 Classical Field Approximation & Effective Interaction Lagrangian

For scalar field masses $m_\varphi \ll 1$ eV, the local phase-space density in the solar neighborhood exceeds 10^{14} quanta per de Broglie wavelength. Under these conditions, quantum fluctuations of the field operator $\hat{\varphi}$ are heavily suppressed, and the field is accurately described by a classical scalar field $\varphi(x,t)$. In the minimal isotropic halo model, the local scalar field at position x and time t is modeled as [3]:

$$\varphi(x,t) = \varphi_0 \cos\big(\omega_\varphi t - \mathbf{k}_\varphi \cdot \mathbf{x} + \theta(t)\big)$$

For a canonically normalised scalar field, the relation $\rho_\varphi \approx \frac{1}{2} m_\varphi^2 \varphi_0^2$ applies in natural units if this species accounts for the assumed local density. The field amplitude therefore depends on an assumed local halo density, and is not a measured QREC-MRT quantity. The velocity-dependent frequency and coherence-time expressions are approximate and depend on the adopted halo model [3, 4].

The interaction between the ultralight scalar field φ and standard model fields is parameterised by an effective interaction Lagrangian $\mathcal{L}_{\text{int}}$ that couples φ linearly to the electromagnetic field tensor $F_{\mu\nu}$, the electron mass m_e, and the nucleon/quark masses m_N [21]:

$$\mathcal{L}_{\text{int}} = -\left(\frac{g_e}{\Lambda^*}\right)\varphi m_e \bar{\psi}_e \psi_e + \left(\frac{g_\gamma}{4\Lambda^*}\right)\varphi F_{\mu\nu}F^{\mu\nu} - \left(\frac{g_N}{\Lambda^*}\right)\varphi m_N \bar{\psi}_N \psi_N$$

Here g_e, g_γ and g_N are model-specific effective couplings whose dimensional interpretation depends on the selected field normalisation. Λ^* is an interaction-scale parameter and is not fixed by the experiment. Matching effective couplings to variations of α and particle-mass ratios requires a consistent nuclear and electromagnetic convention [21].

$$\frac{\delta\alpha(t)}{\alpha_0} = d_{de}\frac{\varphi(t)}{M_{\text{Pl}}}, \quad \frac{\delta\mu(t)}{\mu_0} = \left(d_{m_e} - d_{m_q}\right)\frac{\varphi(t)}{M_{\text{Pl}}}$$

where d_{de}, d_{m_e}, and d_{m_q} represent normalised dilaton coupling parameters. Consequently, any physical observable ν_i (such as an optical clock transition frequency, a quartz crystal mechanical resonance, or a cryogenic optomechanical cavity mode) undergoes fractional modulation:

$$\frac{\delta\nu_i(t)}{\nu_{i,0}} = K_{i,\alpha}\left(\frac{\delta\alpha(t)}{\alpha_0}\right) + K_{i,\mu}\left(\frac{\delta\mu(t)}{\mu_0}\right)$$

where $K_{i,\alpha} = \partial \ln \nu_i / \partial \ln \alpha$ and $K_{i,\mu} = \partial \ln \nu_i / \partial \ln \mu$ are the dimensionless material transition sensitivity coefficients characteristic of the specific atomic transition, electronic structures, or mechanical properties.

2.2 Mechanical Resonator Dynamics & Stochastic Wavefield Modelling

When probing ultralight fields using mechanical resonators, including high-Q quartz crystals, silicon nitride membranes and cryogenic optomechanical accelerometers, scalar-field-induced variations in fundamental constants may produce resonance-frequency modulation or effective mechanical driving, depending on the interaction model, material properties and sensor geometry. For a mechanical mode with effective mass M, resonance frequency $\omega_0 = 2\pi f_0$, and intrinsic mechanical damping rate $\Gamma = \omega_0/Q$, the mechanical displacement $q(t)$ satisfies the stochastic differential equation [24, 25]:

$$Mq''(t) + M\Gamma q'(t) + M\omega_0^2 q(t) = F_{\text{cal}}(t) + F_\varphi(t) + F_n(t)$$

The calibration force $F_{\text{cal}}(t)$ is imposed and independently measured. $F_n(t)$ represents noise. For a classical mechanical oscillator in equilibrium, the one-sided thermal force-noise spectrum can be written $S_F(f) = 4k_B TM\Gamma$ under the stated viscous-damping convention. A hypothetical scalar drive $F_\varphi(t)$ must be derived from the chosen coupling and sensor geometry rather than assumed proportional to the second time derivative of φ. A spatially uniform fundamental-constant modulation may shift resonance frequency instead of generating a centre-of-mass force [24].

$$\chi_q(\omega) = [M(\omega_0^2 - \omega^2 + i\Gamma\omega)]^{-1}$$

The coherence time of a virialised ultralight bosonic field decreases with increasing oscillation frequency. Figure 3 illustrates this dependence using the approximate scaling $\tau_{\text{coh}} \sim 10^6/f_\varphi$, assuming a characteristic Galactic velocity dispersion of $10^{-3}c$ [3, 4].

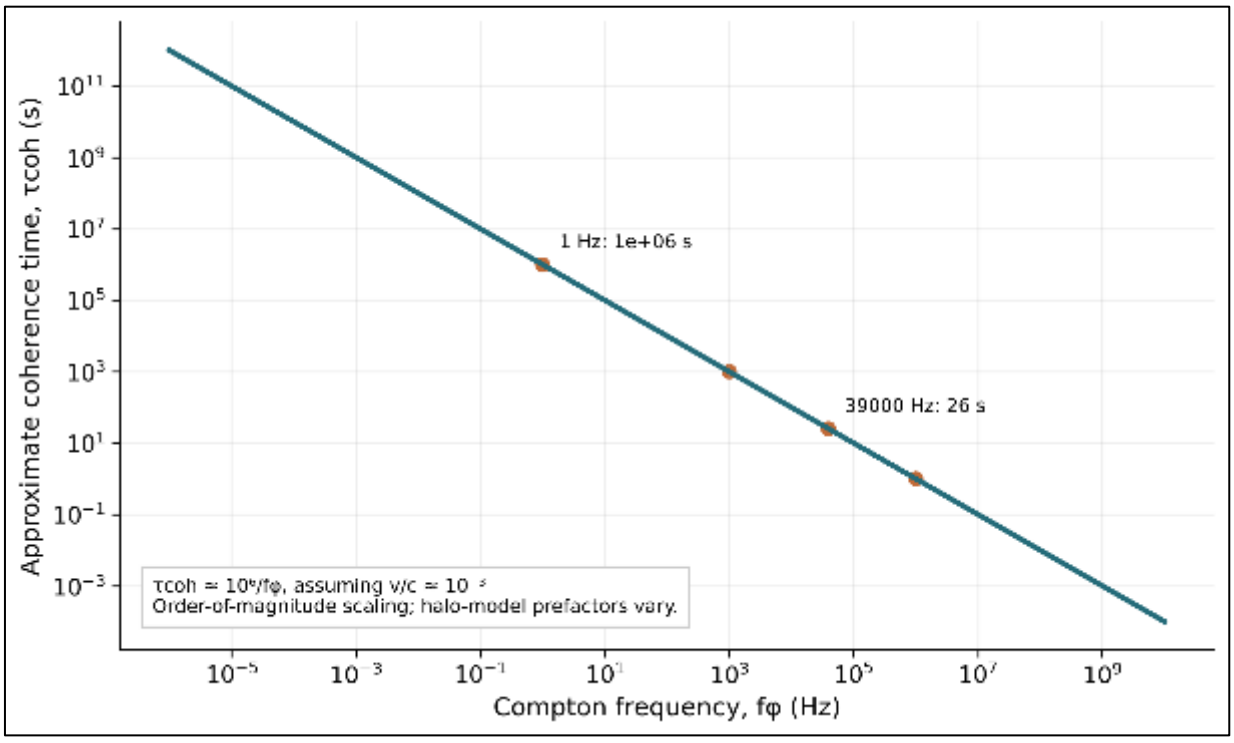


Figure 3: Theoretical coherence-time dependence on ultralight-field oscillation frequency, calculated using $\tau_{\text{coh}} \sim 10^6/f_\varphi$ for a characteristic Galactic velocity of $10^{-3}c$. Numerical prefactors depend on the adopted halo velocity distribution and coherence convention [3, 4].

To accurately model extended observation times $T > \tau_{\text{coh}}$, the ideal monochromatic model of Equation must be expanded to account for the stochastic nature of the galactic dark matter halo. The scalar field is more accurately represented as a superposition of a large number N_m of independent plane wave modes with random phases θ_m and velocities $\mathbf{v}_m$ drawn from a boosted Maxwell-Boltzmann distribution $f(v)$ [4]:

$$\varphi(\mathbf{x},t)=\sum_{m=1}^{N_m}\varphi_m\cos(\omega_m t-\mathbf{k}_m\cdot\mathbf{x}+\theta_m)$$

As a result of this superposition, the local field amplitude $a_\varphi=\sqrt{\varphi(t)^2+\varphi_{\text{quad}}(t)^2}$ is not constant but fluctuates stochastically according to a Rayleigh distribution $P(a_\varphi)=\left(\frac{a_\varphi}{\sigma_\varphi^2}\right)\exp\left(-\frac{a_\varphi^2}{2\sigma_\varphi^2}\right)$, with exponential power coherence decay on timescales exceeding τ_{coh}. Any rigorous signal extraction filter must account for these stochastic amplitude drops to avoid premature signal rejection.

2.3 Multi-Material Fourier Response & Matrix Identifiability

Consider an experimental array consisting of N heterogeneous sensor channels operating simultaneously across a shared observation time T. In the Fourier domain, the discrete frequency response vector $\mathbf{y}(f)\in\mathbb{C}^N$ across the N channels is expressed as:

$$\mathbf{y}(f)=\mathbf{K}(f)\mathbf{d}(f)+\mathbf{B}(f)\mathbf{z}(f)+\boldsymbol{\varepsilon}(f),\quad E[\boldsymbol{\varepsilon}]=0,\quad \text{Cov}(\boldsymbol{\varepsilon})=\boldsymbol{\Sigma}(f)$$

where $\mathbf{K}(f)\in\mathbb{C}^{N\times P}$ is the target material sensitivity matrix containing the pre-calculated sensitivity coefficients $K_{i,\alpha}$ and $K_{i,\mu}$ for P distinct coupling constants $\mathbf{d}(f)\in\mathbb{C}^P$; $\mathbf{B}(f)\in\mathbb{C}^{N\times R}$ is the environmental design matrix mapping R measured nuisance channels $\mathbf{z}(f)\in\mathbb{C}^R$ (e.g., magnetometers, seismometers, temperature sensors, tiltmeters) onto the sensor array; and $\boldsymbol{\varepsilon}(f)\in\mathbb{C}^N$ is the residual stationary Gaussian sensor noise vector with Hermitian positive-definite noise covariance matrix $\boldsymbol{\Sigma}(f)=E[\boldsymbol{\varepsilon}(f)\boldsymbol{\varepsilon}^H(f)]$.

To uniquely isolate the P target scalar field couplings $\mathbf{d}(f)$ from the R environmental nuisance modes $\mathbf{z}(f)$, the combined design matrix $\mathbf{A}=[\mathbf{K}\quad\mathbf{B}]\in\mathbb{C}^{N\times(P+R)}$ must satisfy the necessary rank identifiability condition:

$$\text{rank}([\mathbf{K}\quad\mathbf{B}])-\text{rank}(\mathbf{B})=P$$

However, in realistic physical arrays utilizing similar material substrates, the columns of $\mathbf{K}$ may become near-collinear, causing the matrix $\mathbf{A}^H\boldsymbol{\Sigma}^{-1}\mathbf{A}$ to become severely ill-conditioned. To assess numerical stability and quantify the susceptibility of coupling estimation to noise amplification, we introduce the noise-weighted condition number κ:

$$\kappa=\frac{\sigma_{\max}\left(\boldsymbol{\Sigma}^{-1/2}\mathbf{A}\right)}{\sigma_{\min}\left(\boldsymbol{\Sigma}^{-1/2}\mathbf{A}\right)}$$

The ratio of maximum to minimum singular values of the whitened design matrix is a conditioning diagnostic, not a guarantee of stability. Any κ threshold should be declared before analysis and justified by instrument-specific calibration and acceptable estimator variance; $\kappa<100$ is not a universal physical requirement.

2.4 Linearly Constrained Minimum-Variance (LCMV) Estimator & Calibration Error Propagation

To reconstruct a specific scalar coupling target $s(f)=\mathbf{c}^T\mathbf{d}(f)$ while maintaining complete mathematical orthogonality to all R measured nuisance modes, we construct a Linearly Constrained Minimum-Variance (LCMV) spatial filter weight vector $\mathbf{w}\in\mathbb{C}^N$. The optimal weight vector $\mathbf{w}$ minimises the output variance $\mathbf{w}^H\boldsymbol{\Sigma}\mathbf{w}$ subject to the linear constraint $\mathbf{A}^H\mathbf{w}=\mathbf{c}$, where $\mathbf{c}=(1,0,\dots,0)^T\in\mathbb{R}^{P+R}$:

$$\mathbf{w}=\boldsymbol{\Sigma}^{-1}\mathbf{A}(\mathbf{A}^H\boldsymbol{\Sigma}^{-1}\mathbf{A})^{-1}\mathbf{c},\quad \hat{s}=\mathbf{w}^H\mathbf{y},\quad \text{Var}(\hat{s})=\mathbf{c}^H(\mathbf{A}^H\boldsymbol{\Sigma}^{-1}\mathbf{A})^{-1}\mathbf{c}$$

Equivalently, defining the nuisance-orthogonal projection operator $\mathbf{P}_\perp=\mathbf{I}-\mathbf{B}(\mathbf{B}^H\boldsymbol{\Sigma}^{-1}\mathbf{B})^{-1}\mathbf{B}^H\boldsymbol{\Sigma}^{-1}$, the projected Fisher information matrix $\mathbf{F}\in\mathbb{C}^{P\times P}$ governing target field parameter estimation is expressed as:

$$\mathbf{P}_\perp=\mathbf{I}-\mathbf{B}(\mathbf{B}^H\boldsymbol{\Sigma}^{-1}\mathbf{B})^{-1}\mathbf{B}^H\boldsymbol{\Sigma}^{-1},\quad \mathbf{F}=\mathbf{K}^H\boldsymbol{\Sigma}^{-1}\mathbf{P}_\perp\mathbf{K}$$

In practical experimental metrology, the material sensitivity matrix $\mathbf{K}$ is not known with infinite precision but is estimated with calibration error $\widehat{\mathbf{K}}=\mathbf{K}+\Delta\mathbf{K}$, where $\Delta\mathbf{K}$ is a random calibration error matrix with zero mean and covariance $\text{Cov}(\Delta\mathbf{K})$. Substituting $\widehat{\mathbf{K}}$ the perturbed material-sensitivity matrix into the estimator yields a calibration-uncertainty variance expansion incorporating measurement noise and material-response uncertainty:

$$\text{Var}_{\text{total}}(\hat{s})=\mathbf{c}^H(\mathbf{A}^H\boldsymbol{\Sigma}^{-1}\mathbf{A})^{-1}\mathbf{c}+\mathbf{w}^H E\left[\Delta\mathbf{K}\hat{\mathbf{d}}\hat{\mathbf{d}}^H\Delta\mathbf{K}^H\right]\mathbf{w}$$

Accounting for calibration variance prevents the system from reporting unrealistically narrow confidence intervals when processing high-signal-to-noise ratio calibration injections.

2.5 QREC-MRT Intervention Architecture & Three-Tier Epistemological Framework

To evaluate Quantum-Resonant Energy Coupling–Molecular Resonance Technology (QREC-MRT), the study proposes independently scheduled, randomised and blinded active ($a = 1$) and sham ($a = 0$) states. The physical implementation and relevant energy exchanges must be disclosed sufficiently for replication. Neither the existence of an active driver nor a specific optical, acoustic or electromagnetic actuation mechanism is assumed without device documentation.

To evaluate whether an active intervention produces instrument-level variance reduction, we define the input-referred active-versus-sham contrast ratio J and its corresponding log-variance metric L:

$$J = \frac{\mathrm{Var}(\hat{s} \mid a = 1)}{\mathrm{Var}(\hat{s} \mid a = 0)}, \quad L = \log J$$

A reproducible negative log variance ratio L would indicate lower measured variance under active than sham acquisition for the specified apparatus, but would not independently identify a cosmological field. The following three-tier classification separates instrument-level performance, field-model consistency and independent validation. Thresholds must be pre-registered using a justified statistical power analysis.

- **Tier A (Instrument Metrology):** Requires demonstrating statistically significant input-referred noise variance reduction ($L < 0$, with predeclared statistical criteria) under a randomised, double-blind active vs sham contrast, accompanied by complete calibration recovery.
- **Tier B (Model Alignment):** Requires that the residual vector $\mathbf{r} = \mathbf{y} - \mathbf{Bz}$ aligns with the pre-declared, material-dependent theoretical signature vector $\mathbf{t}$ ($C_{\mathrm{fp}} = \frac{|\mathbf{t}^H \mathbf{r}|^2}{(\mathbf{t}^H \mathbf{t})(\mathbf{r}^H \mathbf{r})} > C_{\mathrm{thresh}}$) with statistically justified suppression of characterised environmental nuisance contributions and quantitative assessment of residual interference
- **Tier C (Cosmological Discovery):** Requires spatial cross-coherence $S_{AB}(f) > 0$ across independent geographically separated laboratories (baseline selected using the predicted coherence length), global trial-count corrections (look-elsewhere effect), and third-party replication.

The sequential assessment of instrument performance, model-specific signature consistency and independent experimental validation is illustrated in Figure 4.

The proposed heterogeneous sensor architecture is designed to combine cryogenic optomechanical accelerometers, silicon cavity resonators and optical atomic clocks through nuisance-orthogonal estimation. Its achievable input-referred sensitivity will depend on independently calibrated transfer functions, sensor-noise covariance and measurement bandwidth. The published benchmarks in Table 1 provide reference performance levels but do not establish the sensitivity of the proposed integrated QREC-MRT configuration.

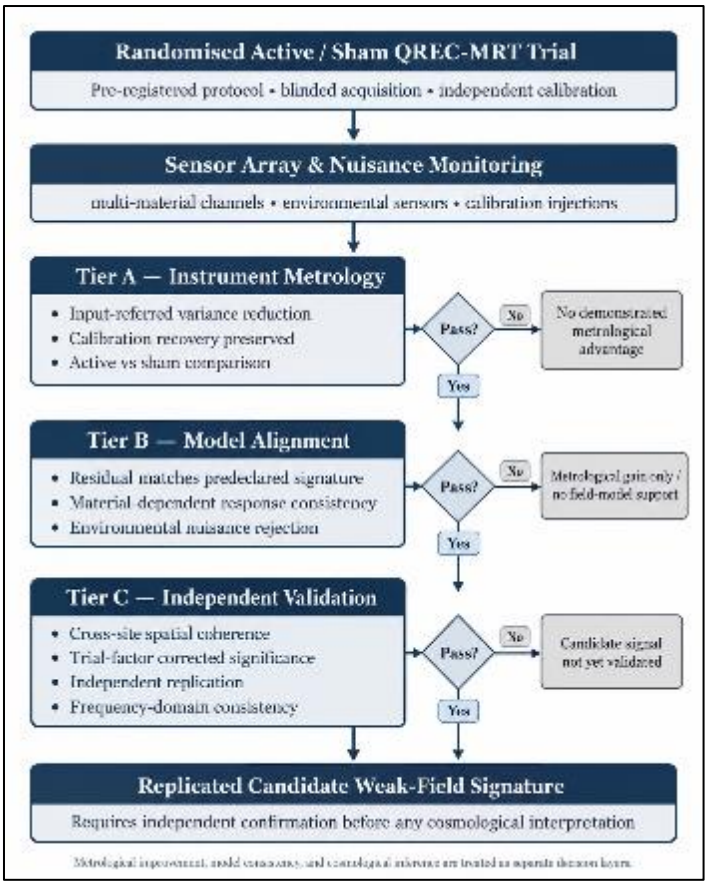


Figure 4: Proposed three-tier QREC-MRT validation framework, comprising Tier A (instrument metrology), Tier B (model-specific signal alignment) and Tier C (independent spatial and experimental verification). Author-developed methodological framework.

3 PUBLISHED BENCHMARKS AND PROSPECTIVE SENSITIVITY ANALYSIS

3.1 External Observational Benchmarks & Multi-Channel Sensitivity

To ground our theoretical signal model and multi-material response matrices in realistic physical parameters, we benchmark our interrogation architecture against published state-of-the-art cosmological measurements, cryogenic optomechanical accelerometers, and ultrastable optical frequency networks. Table 1 summarizes these external benchmarks, detailing their physical observables, target mass-frequency bands, baseline sensitivity limits, and corresponding roles within the three-tier metrological framework.

Table 1: Published cosmological and precision-metrology benchmarks relevant to the proposed QREC-MRT multi-material resonance investigation [1, 10,11].

Benchmark / Source	Physical Observable	Baseline Noise Floor / Stability	Metrological / Cosmological Role
Planck 2018 Results (A&A 641, A6)	CDM Density $\Omega_c h^2$ Hubble Constant H_0	0.120 ± 0.001 67.4 ± 0.5 km/s/Mpc	Cosmological density fractions; does not set local halo density
Dey Chowdhury et al. (2026) (PRD 113, L121303)	Optomechanical Accel. Compton Freq. f_0 = 39 kHz	10 ng_0 / √Hz (m_φ = 1.61 × 10^{-10} eV)	Resonant acceleration noise floor for high-Q mechanical channels
Schioppo et al. (2022) (Nat. Commun. 13, 212)	Optical Fiber Network Baseline L = 2,220 km	7 × 10^{-17} Instability (30–200 s averaging time)	Long-baseline optical-frequency stability and distributed metrology benchmark

3.2 Sensitivity Limits & Input-Referred Noise Spectral Density

The proposed application of linearly constrained minimum-variance (LCMV) estimation to a heterogeneous sensing architecture incorporating cryogenic optomechanical accelerometers, silicon optical cavity resonators and atomic frequency references provides a theoretical basis for integrating material-dependent responses while suppressing independently characterised environmental interference. The achievable input-referred sensitivity spectrum, $S_{a,\mathrm{ref}}(f)$, depends on the calibrated transfer functions, sensor-noise covariance matrices, material sensitivity coefficients and frequency-dependent correlations between measurement channels.

As an experimentally established benchmark, a cryogenic cavity optomechanical accelerometer employing a silicon nitride membrane mounted on a 4 K platform demonstrated a tunable mechanical resonance near 39 kHz and an acceleration amplitude spectral density of approximately $10\ \mathrm{ng_0\ Hz^{-1/2}}$ over a 30 Hz frequency interval near resonance. This sensitivity was achieved through a combination of shot-noise-limited displacement readout, radiation-pressure feedback cooling and controlled mechanical resonance tuning [11]. The corresponding thermal force-noise spectral density, under the classical viscous-damping approximation, is given by:

$$S_F^{\mathrm{th}} = 4k_B T M \Gamma$$

where k_B is Boltzmann's constant, T is the mechanical bath temperature, M is the effective resonator mass and $\Gamma = \omega_0/Q$ is the mechanical damping rate.

Within the proposed QREC-MRT-inspired multi-material interrogation framework, these experimentally established parameters provide a reference for evaluating resonance-selective sensitivity, calibration stability and nuisance-orthogonal signal reconstruction. The resulting integrated measurement sensitivity can be determined through prospective calibration and differential analysis, thereby providing a quantitative basis for assessing the potential contribution of QREC-MRT to precision weak-field metrology. The noise-weighted estimator provides a testable methodology for suppressing characterised seismic, thermal and electromagnetic disturbances. The effectiveness of nuisance rejection depends on calibrated sensor responses, noise-covariance estimation and the presence of unmodelled interference. The independent experimental benchmarks presented in Table 1 establish reference performance characteristics but do not independently demonstrate QREC-MRT-specific sensitivity enhancements. Accordingly, future randomised, blinded active-versus-sham trials should quantify input-referred variance ratios with associated confidence intervals, verify signal recovery using independent calibration injections and report calibrated transfer functions across the relevant measurement bandwidth.

3.3 Quantitative Benchmark Analysis and Implications for QREC-MRT

The published optomechanical and optical-frequency measurements examined in Sections 3.1 and 3.2 establish experimentally demonstrated reference parameters for evaluating the QREC-MRT Multi-Material Differential Resonance Framework. Building upon these benchmarks, the present analysis examines their implications for ultralight-field frequency correspondence, heterogeneous sensor integration, coupling identifiability, and calibration-preserving measurement assessment.

3.3.1 Quantitative Frequency Correspondence and Metrological Implications

The optomechanical resonator operating near 39 kHz, reported by Dey Chowdhury et al. [11], provides a reference frequency for examining ultralight-field resonance characteristics. Using the Compton energy–frequency relationship,

$$E_\phi = m_\phi c^2 = h f_\phi,$$

the corresponding field rest energy is

$$E_\phi \approx 1.61 \times 10^{-10}\ \mathrm{eV}.$$

This relationship establishes the frequency–energy correspondence relevant to the resonance-based investigation described in Section 2.2 and illustrated in Figure 2.

The published optical-frequency comparison by Schioppo et al. [10], demonstrating fractional-frequency instability near 7×10^{-17} across a 2,220 km optical-fibre network, provides a complementary reference for distributed frequency stability and spatially separated sensing.

These benchmarks represent distinct physical observables. Their use within a common multi-material estimation framework therefore requires independently calibrated response coefficients, appropriate dimensional normalisation,

and characterisation of sensor-specific noise covariance. The combination of heterogeneous measurement channels is meaningful only when their coupling responses are sufficiently distinguishable after accounting for environmental disturbances.

3.3.2 Methodological Differentiation and Integrated Measurement Architecture

The QREC-MRT framework integrates material-dependent resonance interrogation, coupling-specific response modelling, nuisance-orthogonal estimation, and state-dependent sensitivity analysis within a unified metrological architecture. Table 2 compares this integration with selected established precision-sensing methodologies. The comparison concerns the organisation of measurement and validation procedures rather than experimentally demonstrated superiority.

Table 2: Comparison of established precision-sensing methodologies and their integration within the QREC-MRT Multi-Material Differential Resonance Framework.

Evaluation criterion	Established precision-sensing approaches	QREC-MRT framework
Sensor architecture	Individual resonators, atomic clocks, and differential sensor networks	Integrated heterogeneous multi-material resonance interrogation
Coupling identification	Interaction-specific observables and calibrated sensor responses	Noise-weighted multi-material coupling-identifiability analysis
Environmental interference	Instrument-specific noise mitigation and differential compensation	Nuisance-orthogonal estimation using characterised disturbance channels
Calibration	Instrument-specific transfer-function calibration and uncertainty assessment	Calibration-preserving active-versus-sham interrogation and response verification
Sensitivity assessment	Instrument noise floors, statistical estimation, and uncertainty analysis	Projected Fisher-information assessment and state-dependent information comparison
Validation	Model-specific controls, statistical testing, and independent replication	Integrated three-tier assessment of instrument performance, coupling-signature agreement, and spatial-coherence verification

The comparison identifies the distinguishing organisational features of the QREC-MRT methodology. Established sensing techniques may incorporate several of these elements individually or in combination. The contribution examined here is their joint formulation within a state-dependent, multi-material interrogation and validation architecture.

3.3.3 Principal Methodological Contribution and Scientific Implications

The principal methodological contribution of the QREC-MRT Multi-Material Differential Resonance Framework lies in the integrated assessment of material-dependent coupling identifiability, nuisance-orthogonal signal reconstruction, calibration-preserving state-dependent interrogation, and independent field-signature verification.

A distinguishing feature is the joint evaluation of two essential requirements: whether heterogeneous sensor responses permit reliable discrimination of candidate field-coupling parameters, and whether changes in interrogation conditions improve input-referred measurement information while preserving calibrated material-response signatures.

The combination of noise-weighted conditioning, double-differential material-response analysis, and Fisher-information assessment provides quantitative criteria for addressing these requirements. The three-tier validation architecture further separates instrumental metrological performance, consistency with theoretically predicted coupling signatures, and independent spatial-coherence verification.

This integrated formulation establishes a reproducible and experimentally testable basis for evaluating QREC-MRT-associated resonance interrogation in ultralight-field sensing. Its scientific significance lies in linking material-response diversity, measurement-information integrity, and coupling-specific verification within a common analytical framework, thereby providing a structured foundation for subsequent precision-metrology investigations.

4 DISCUSSION: PROTOCOL SAFEGUARDS & IMPLEMENTATION ANALYSIS

4.1 Protocol Safeguards & Tripartite Dataset Protocol

A critical vulnerability in complex metrological searches is the risk of subtle over-fitting or selection bias when optimising material sensitivity matrices K(f) or environmental nuisance libraries B(f) on the same dataset used for signal identification. To eliminate this risk, experimental evaluations must enforce a strict Tripartite Dataset Protocol:

- **Calibration Dataset:** Acquisition sequences dedicated exclusively to estimating physical sensor-transfer functions, electronic gain characteristics and environmental nuisance-transfer matrices. These data should not be used for confirmatory signal searches.
- **Design Dataset:** Used to evaluate the noise-weighted condition number, compute the projected Fisher-information matrix and select complementary material-channel combinations. All analysis parameters should be fixed before confirmatory evaluation.
- **Confirmatory Dataset:** The dataset should remain blinded and inaccessible until the analysis protocol has been finalised. It is then used to calculate the primary log-variance ratio and evaluate the predefined Tier A, Tier B and Tier C decision statistics.

4.2 Sample Size Planning & Multi-Site Cross-Spectral Coherence

To achieve sufficient statistical power for detecting a target log-variance ratio reduction $\delta = |L_{\text{target}}|$ with significance level α and power $1-\beta$, the required number of independent observation segments n is bounded by:

$$n \gtrsim \left[\frac{(z_{1-\alpha} + z_{1-\beta})\sigma_L}{\delta}\right]^2$$

where z_p is the p-th quantile of the standard normal distribution, and $\sigma_L^2 \approx 2/n_{\text{deg}}$ is the variance of the sample log-variance estimator under Gaussian noise. For multi-site experiments combining geographically separated laboratories (Site A and Site B over baselines > 100 km), shared spatial scalar field signals are distinguished from local environmental noise via the cross-power spectral density $S_{AB}(f)$ and magnitude-squared coherence $\gamma_{AB}^2(f)$:

$$S_{AB}(f) = E[\tilde{y}_A(f)\tilde{y}_B^*(f)], \quad \gamma_{AB}^2(f) = \frac{|S_{AB}(f)|^2}{S_{AA}(f)S_{BB}(f)}$$

Spatial coherence is model- and frequency-dependent. A shared ultralight scalar field may produce correlated responses across geographically separated sensors, depending on the assumed Galactic halo velocity distribution, field coherence length, instrumental transfer functions and separation between measurement sites. The de Broglie wavelength varies inversely with particle mass and characteristic velocity, making the expected spatial correlation dependent on the specific field model and experimental baseline. Consequently, a fixed sensor separation alone neither guarantees nor excludes correlated field signatures. Common timing references, environmental disturbances and instrumental coupling may also generate cross-spectral correlations and must be independently characterised and distinguished from candidate field-induced signals [9].

4.3 Energy Accounting, Causality, & Methodological Scope

Every experimental implementation must document local energy inputs, environmental heating, electromagnetic emissions and any actuation delivered to the sensor. Attenuation or shielding levels must be measured for the particular installation rather than assumed. Non-contact operation does not imply superluminal signalling, unaccounted energy generation or evidence of a new field.

4.4 State-dependent resonance response and protocol identifiability

To distinguish a change in sensor behaviour from a change in a candidate external-field coupling, the measured Fourier response is parameterised independently for the active ($\boldsymbol{a} = \mathbf{1}$) and sham ($\boldsymbol{a} = \mathbf{0}$) acquisition states. The model allows both the target transfer matrix and environmental susceptibility to depend on the intervention, rather than attributing every improvement to suppressed noise.

$$\mathbf{y}_{\boldsymbol{a}}(\boldsymbol{f}) = \mathbf{G}_{\boldsymbol{a}}(\boldsymbol{f})\mathbf{K}_{\mathbf{0}}(\boldsymbol{f})\mathbf{d}(\boldsymbol{f}) + \mathbf{B}_{\boldsymbol{a}}(\boldsymbol{f})\mathbf{z}(\boldsymbol{f}) + \boldsymbol{\varepsilon}_{\boldsymbol{a}}(\boldsymbol{f}), \quad \mathrm{Cov}(\boldsymbol{\varepsilon}_{\boldsymbol{a}}) = \boldsymbol{\Sigma}_{\boldsymbol{a}}(\boldsymbol{f})$$

Here $\mathbf{G}_{\boldsymbol{a}}$ is a calibrated state-dependent transfer operator, $\mathbf{K}_{\mathbf{0}}$ is a precomputed material coupling matrix, $\mathbf{d}$ is a candidate physical field, and $\mathbf{z}$ contains independently monitored disturbances. The intervention effect on $\mathbf{G}_{\boldsymbol{a}}$ is a measurement hypothesis, not an additional field–matter interaction. Without independently establishing $\mathbf{G}_{\boldsymbol{a}}$ through

calibration injection and held-out data, a dark-sector amplitude $\mathbf{d}$ cannot be identified from $\mathbf{G}_a\mathbf{d}$ because the two factors may be confounded.

An explicit state-invariance check follows from a calibration drive $\boldsymbol{u}_{\text{cal}}$ of known amplitude. With calibrated transfer functions $\boldsymbol{H_1}$ and $\boldsymbol{H_0}$, define the normalised signal-recovery ratio as:

$$\boldsymbol{R}_{\text{cal}}(\boldsymbol{f}) = \frac{\hat{\boldsymbol{y}}_{\mathbf{1},\text{cal}}(\boldsymbol{f})/\boldsymbol{H_1}(\boldsymbol{f})}{\hat{\boldsymbol{y}}_{\mathbf{0},\text{cal}}(\boldsymbol{f})/\boldsymbol{H_0}(\boldsymbol{f})}$$

Under correct calibration and no intervention-induced change in injected-signal amplitude, $\boldsymbol{R}_{\text{cal}}$ should be consistent with unity within a predeclared uncertainty interval. An intervention producing lower output variance but materially biased $\boldsymbol{R}_{\text{cal}}$ cannot be described as a demonstrated sensitivity gain. This guards against gain compression, feedback artefacts and bandwidth-dependent filtering, all of which can reduce apparent noise without improving input-referred information.

4.5 Double-differential material contrasts

The proposed QREC-MRT-specific evaluation is strengthened by comparing not just active versus sham states, but their relative response across two distinct sensor compositions or transitions. For independently calibrated fractional-frequency or amplitude residuals $\boldsymbol{y_{i,a}}$, a difference-in-differences contrast can be defined as:

$$\boldsymbol{D_{ij}} = (\bar{\boldsymbol{y}}_{\boldsymbol{i,1}} - \bar{\boldsymbol{y}}_{\boldsymbol{i,0}}) - (\bar{\boldsymbol{y}}_{\boldsymbol{j,1}} - \bar{\boldsymbol{y}}_{\boldsymbol{j,0}})$$

A non-zero $\boldsymbol{D_{ij}}$ is not automatically evidence of a new field: unequal thermal susceptibility, drift, intervention pickup or conventional actuation may produce the same contrast. The value of this design is its falsifiability. A specified scalar coupling predicts a composition-dependent response ratio through $\boldsymbol{K_{i,\alpha}}$ and $\boldsymbol{K_{i,\mu}}$ [21]. Atomic-clock scalar searches provide a physical precedent for testing such coefficient-dependent signatures [7]. A valid comparison must account for correlated uncertainties between sensors, repeated measurements and state order.

If material sensitivity vectors are proportional after nuisance projection, $\boldsymbol{D_{ij}}$ alone cannot separate multiple couplings. The study therefore requires the singular-value spectrum of the whitened response matrix to be reported with uncertainty bounds, not simply a binary rank classification. Preselection using measurements independent of the confirmatory trial reduces overfitting.

4.6 A falsifiable signature-preservation condition

A potentially distinctive methodological outcome would be a repeatable change in effective sensor information that preserves the calibrated material-coupling fingerprint. Let $\boldsymbol{\mathcal{F}_a} = \mathbf{K}_{\boldsymbol{a}}^{\boldsymbol{H}}\boldsymbol{\Sigma}_{\boldsymbol{a}}^{\mathbf{-1}}\mathbf{P}_{\perp,\boldsymbol{a}}\mathbf{K}_{\boldsymbol{a}}$ denote the projected Fisher matrix for state $\boldsymbol{a}$. A dimensionless information-gain criterion for a single prespecified coupling direction $\mathbf{c}$ can be written as:

$$\boldsymbol{\eta_c} = \frac{\left[\mathbf{c}^{\boldsymbol{H}}\boldsymbol{\mathcal{F}}_{\mathbf{1}}^{\mathbf{-1}}\mathbf{c}\right]^{\mathbf{-1}}}{\left[\mathbf{c}^{\boldsymbol{H}}\boldsymbol{\mathcal{F}}_{\mathbf{0}}^{\mathbf{-1}}\mathbf{c}\right]^{\mathbf{-1}}}, \quad \boldsymbol{\eta_c} > \mathbf{1} \text{ indicates greater estimated information}$$

This comparison is meaningful only when the same parameterisation, sensor resources, integration duration and frequency band are used in both conditions. Report $\boldsymbol{\eta_c}$ with uncertainty, coupling-template bias, false-positive rate and calibration recovery. The target information gain must persist on held-out calibration signals and independent experiment days. Existing optical frequency-comparison and distributed-cavity searches provide realistic benchmarks for the required controls [9].

This paper does not claim that the inequalities $\boldsymbol{\eta_c} > \mathbf{1}$ or $\boldsymbol{J} < \mathbf{1}$ have been observed for QREC-MRT. They define pre-registerable outcomes that could demonstrate an instrument-level methodological advantage. Discovery of a fundamental weak-field interaction remains a separate test requiring a physically derived coupling, quantitative spectral prediction and independent replication.

4.7 Limits on novelty and differentiation from established approaches

The LCMV estimator, Fisher information, singular-value conditioning and randomised controls are established mathematical tools. The specific proposed contribution is their predeclared combination into a calibration-preserving, state-dependent, multi-material interrogation design with three separate decision stages: (i) does intervention improve input-referred information, (ii) is any residual consistent with the predicted composition-sensitive template, and (iii) is

a candidate signal independently replicated with a coherent spatial and frequency-domain model? These are testable protocol-level claims, not a new principle of quantum mechanics.

A comparative experiment should include four reporting baselines: a fixed unmodified sensor; the same sensor with conventional optimised feedback; a sham QREC-MRT activation; and the active QREC-MRT state. Without the conventional-feedback comparator, any apparent advantage cannot be attributed specifically to the proposed intervention. Existing mechanical scalar-field concepts [24] and optomechanical accelerometer searches [11] provide relevant prior experimental architecture for this comparison.

A negative result is equally interpretable: absence of information gain after calibration controls rules out the claimed metrological improvement at the tested sensitivity. A reproducible intervention gain without a coupling-specific signature supports improved sensing only. A coupling-like residual without independent interference rejection is inconclusive. No scenario warrants claiming dark-matter detection from variance reduction alone.

5 CONCLUSION

This research establishes a mathematically defined Multi-Material Differential Resonance Framework extending Quantum-Resonant Energy Coupling–Molecular Resonance Technology (QREC-MRT) into ultralight-field investigations and precision quantum metrology. Building upon QREC-MRT's ongoing operational development and cross-sector evaluations, the study integrates heterogeneous material-response characteristics, resonance-selective interrogation, calibrated sensor-transfer functions and coupling-specific statistical estimation within a unified analytical architecture.

The framework establishes matrix-rank and noise-weighted conditioning criteria for coupling identifiability, supported by nuisance-orthogonal signal reconstruction and calibration-uncertainty propagation. Double-differential material-response comparisons and Fisher-information-based assessment provide quantitative criteria for evaluating state-dependent changes in measurement sensitivity while preserving calibrated material-coupling signatures.

The principal novelty lies in the joint assessment of material-dependent coupling identifiability, state-dependent measurement-information gain and calibration integrity within a QREC-MRT-based multi-material resonance architecture. By integrating these requirements with active-versus-sham interrogation and nuisance-orthogonal estimation, the framework provides a coherent methodology for distinguishing changes in instrumental performance from candidate field-coupling signatures. This integrated approach constitutes the specific methodological contribution of the study, rather than the individual mathematical techniques employed.

A three-tier validation architecture further distinguishes instrumental metrological performance, agreement with theoretically predicted material-dependent coupling signatures and independent spatial-coherence verification. The quantitative assessment of published optomechanical and optical-frequency metrology benchmarks establishes experimentally grounded reference parameters for instrument selection, calibration planning and future comparative investigations.

Together, these contributions establish a reproducible and experimentally testable analytical framework for assessing the application of QREC-MRT to ultralight scalar-field interactions, fundamental-constant variations and distributed precision metrology. The framework provides a basis for independent experimental evaluation while maintaining the distinction between established instrumental capabilities and the verification of field-specific interactions.

5.1 Study Classification and Reproducibility

This study constitutes an original theoretical and methodological extension of QREC-MRT into ultralight-field sensing and precision quantum metrology. QREC-MRT is undergoing operational evaluation across multiple application sectors, while the present investigation develops the mathematical and metrological framework for assessing its application to precision weak-field sensing. These operational evaluations are distinct from direct experimental verification of ultralight-field interactions.

The analysis incorporates established physical models, published optomechanical and optical-frequency measurements, and mathematically defined relationships for material-dependent coupling responses. The material-response, environmental nuisance and noise-covariance matrices are specified within a generalised measurement model, with instrument-specific parameters to be established through independent calibration.

The resulting analytical relationships, coupling-identifiability conditions, uncertainty-assessment procedures and three-tier validation criteria provide a reproducible foundation for computational evaluation and experimental investigation of QREC-MRT-associated resonance responses.

STATEMENTS ON COMPLIANCE WITH ETHICAL STANDARDS

Acknowledgments

The author acknowledges the contributions of the scientific community whose published research in ultralight-field physics, quantum metrology, optomechanical sensing and statistical estimation provided the theoretical foundations and reference benchmarks. The author also acknowledges the use of AI-assisted tools for manuscript structuring, language refinement and editorial review. All scientific interpretations, mathematical formulations, technical conclusions and final manuscript content remain the responsibility of the author.

Disclosure of conflict of interest

The author is associated with TechnoPilot Quantum Labs and serves as Chief Executive Officer of TOL Biotech USA. The author has research and commercial interests in QREC-MRT and its potential applications in resonance-based sensing and precision metrology. These interests are disclosed in the interests of scientific transparency.

Analytical Calculations and Figure Provenance

All analytical calculations and graphical representations in this study are based on established physical principles, mathematical formulations and independently published scientific findings. Figure 1 presents the cosmological energy-density composition derived from the Planck 2018 central parameter estimates [1]. Figure 2 illustrates the calculated relationship between ultralight-field rest energy and Compton oscillation frequency, incorporating the published optomechanical resonator frequency as a reference benchmark [11]. Figure 3 presents the theoretical relationship between ultralight-field oscillation frequency and coherence time under the adopted Galactic velocity-dispersion assumptions [3, 4]. Figure 4 depicts the author-developed three-tier QREC-MRT validation architecture. All figures serve explanatory, comparative or methodological purposes and do not constitute experimental verification of ultralight-field interactions. The analytical relationships are reproducible from the equations, physical constants, published benchmarks and stated assumptions provided in the manuscript.

Data Availability

This study is theoretical and methodological, drawing upon publicly available scientific literature, published experimental benchmarks and established physical constants. No new experimental datasets were generated specifically for this investigation. The mathematical formulations, analytical relationships, relevant input parameters and supporting references required to evaluate the theoretical findings are provided in the manuscript. No separate experimental dataset is associated with this study.

REFERENCES

[1] Planck Collaboration (2020). Planck 2018 results VI. Cosmological parameters. Astronomy & Astrophysics 641, A6. DOI: https://doi.org/10.1051/0004-6361/201833910

[2] Clowe D et al. (2006). A direct empirical proof of the existence of dark matter. Astrophysical Journal Letters 648, L109. DOI: https://doi.org/10.1086/508162

[3] Marsh DJE (2016). Axion cosmology. Physics Reports 643, 1. DOI: https://doi.org/10.1016/j.physrep.2016.06.005

[4] Centers GP et al. (2021). Stochastic fluctuations of bosonic dark matter. Nature Communications 12, 7321. DOI: https://doi.org/10.1038/s41467-021-27632-7

[5] Weinberg S (1978). A new light boson? Physical Review Letters 40, 223. DOI: https://doi.org/10.1103/PhysRevLett.40.223

[6] Wilczek F (1978). Problem of strong P and T invariance in the presence of instantons. Physical Review Letters 40, 279. DOI: https://doi.org/10.1103/PhysRevLett.40.279

[7] Arvanitaki A, Huang J & Van Tilburg K (2015). Searching for dilaton dark matter with atomic clocks. Physical Review D 91, 015015. DOI: https://doi.org/10.1103/PhysRevD.91.015015

[8] Van Tilburg K et al. (2015). Search for ultralight scalar dark matter with atomic spectroscopy. Physical Review Letters 115, 011802. DOI: https://doi.org/10.1103/PhysRevLett.115.011802

[9] Filzinger M et al. (2025). Ultralight dark matter search with space-time separated atomic clocks and cavities. Physical Review Letters 134, 031001. DOI: https://doi.org/10.1103/PhysRevLett.134.031001

[10] Schioppo M, Kronjäger J, Silva A et al. (2022). Comparing ultrastable lasers at 7×10^{-17} fractional frequency instability through a 2220 km optical fibre network. Nature Communications 13, 212. DOI: https://doi.org/10.1038/s41467-021-27884-3

[11] Dey Chowdhury M, Manley JP, Condos CA, Agrawal AR & Wilson DJ (2026). Optomechanical accelerometer search for ultralight dark matter. Physical Review D 113, L121303. DOI: https://doi.org/10.1103/16yd-qj5v

[12] Rubin VC & Ford WK (1970). Rotation of the Andromeda Nebula. Astrophysical Journal 159, 379. DOI: https://doi.org/10.1086/150317

[13] Rubin VC (1983). The rotation of spiral galaxies. Science 220, 1339–1344. DOI: https://doi.org/10.1126/science.220.4604.1339

[14] Bertone G, Hooper D & Silk J (2005). Particle dark matter: Evidence, candidates and constraints. Physics Reports 405, 279. DOI: https://doi.org/10.1016/j.physrep.2004.08.031

[15] Feng JL (2010). Dark matter candidates from particle physics and methods of detection. Annual Review of Astronomy and Astrophysics 48, 495. DOI: https://doi.org/10.1146/annurev-astro-082708-101659

[16] Peccei RD & Quinn HR (1977). CP conservation in the presence of pseudoparticles. Physical Review Letters 38, 1440. DOI: https://doi.org/10.1103/PhysRevLett.38.1440

[17] Preskill J, Wise MB & Wilczek F (1983). Cosmology of the invisible axion. Physics Letters B 120, 127. DOI: https://doi.org/10.1016/0370-2693(83)90637-8

[18] Abbott LF & Sikivie P (1983). A cosmological bound on the invisible axion. Physics Letters B 120, 133. DOI: https://doi.org/10.1016/0370-2693(83)90638-X

[19] Dine M & Fischler W (1983). The not-so-harmless axion. Physics Letters B 120, 137. DOI: https://doi.org/10.1016/0370-2693(83)90639-1

[20] Sikivie P (1983). Experimental tests of the invisible axion. Physical Review Letters 51, 1415. DOI: https://doi.org/10.1103/PhysRevLett.51.1415

[21] Damour T & Donoghue JF (2010). Equivalence principle violations and couplings of a light dilaton. Physical Review D 82, 084033. DOI: https://doi.org/10.1103/PhysRevD.82.084033

[22] Damour T, Piazza F & Veneziano G (2002). Violations of the equivalence principle in a dilaton-runaway scenario. Physical Review D 66, 046007. DOI: https://doi.org/10.1103/PhysRevD.66.046007

[23] Derevianko A & Pospelov M (2014). Hunting for topological dark matter with atomic clocks. Nature Physics 10, 933. DOI: https://doi.org/10.1038/nphys3137

[24] Arvanitaki A, Dimopoulos S & Van Tilburg K (2016). Sound of dark matter: Searching for light scalars with resonant-mass detectors. Physical Review Letters 116, 031102. DOI: https://doi.org/10.1103/PhysRevLett.116.031102

[25] Graham PW et al. (2016). Dark matter direct detection with accelerometers. Physical Review D 93, 075029. DOI: https://doi.org/10.1103/PhysRevD.93.075029

[26] Arvanitaki A et al. (2018). Search for light scalar dark matter with atomic gravitational wave detectors. Physical Review D 97, 075020. DOI: https://doi.org/10.1103/PhysRevD.97.075020

[27] Manley J et al. (2021). Searching for vector dark matter with an optomechanical accelerometer. Physical Review Letters 126, 061301. DOI: https://doi.org/10.1103/PhysRevLett.126.061301

[28] Kobayashi T et al. (2022). Search for ultralight dark matter from long-term frequency comparisons of optical and microwave atomic clocks. Physical Review Letters 129, 241301. DOI: https://doi.org/10.1103/PhysRevLett.129.241301

[29] Zhang X et al. (2023). Search for ultralight dark matter with spectroscopy of radio-frequency atomic transitions. Physical Review Letters 130, 251002. DOI: https://doi.org/10.1103/PhysRevLett.130.251002

[30] Brzeminski D & Pierce A (2026). Searching for ultralight scalar dark matter with clocks in Low Earth Orbit. JHEP 2026, 161. DOI: https://doi.org/10.1007/JHEP08(2026)161

[31] Baker CG, Bowen WP, Cox P, Dolan MJ, Goryachev M & Harris G (2024). Optomechanical dark matter instrument for direct detection. Physical Review D 110, 043005. DOI: https://doi.org/10.1103/PhysRevD.110.043005

[32] Raffelt GG (2008). Astrophysical axion bounds. Lecture Notes in Physics 741, 51–71. DOI: https://doi.org/10.1007/978-3-540-73518-2_3

[33] de Swart JG, Bertone G & van Dongen J (2017). How dark matter came to matter. Nature Astronomy 1, 0059. DOI: https://doi.org/10.1038/s41550-017-0059